Radial Flux Leakage Integrated Quasi-3D Approach for Accurate Axial Flux PM Motor Analysis

Younjae Hwang[1], Ki-O Kim[2], Won-Seok Cha[1], Byeong-Cheol Bae[1], Jae-Hyeon Kim[1], and Myung-Seop Lim[2]

[1]Department of Automotive Engineering (Automotive-Computer Convergence), Hanyang University, Seoul 04763, Republic of Korea
[2]Department of Automotive Engineering, Hanyang University, Seoul 04763, Republic of Korea

Axial flux permanent magnet (AFPM) motors have drawn significant attention due to their compact size, high torque density, and broad applicability. However, accurately designing an AFPM motor requires computationally intensive 3-D finite element analysis (3D FEA) owing to its topology. To alleviate this, a quasi-3-D (quasi-3D) model can be employed, in which the AFPM motor's geometry is divided in the radial direction and represented in a flattened, 2-D equivalent form. The quasi-3D model offers an efficient alternative, but it typically fails to consider important factors, such as radial flux leakage. This limitation can result in discrepancies between the predicted voltage and torque and those obtained from 3D FEA results. In this article, we improve the conventional quasi-3D model by calculating the radial leakage path's permeance and incorporating it into the 2-D analysis. As a result, the improved quasi-3D model exhibits a better correlation with 3D FEA than the conventional quasi-3D model with a higher division. The improved quasi-3D model significantly reduces computational cost with minimal sacrifice of precision compared to 3D FEA, enabling faster and more reliable design processes.

***Index Terms*— 3-D finite element analysis (3D FEA), axial flux permanent magnet (AFPM), permeance, quasi-3D model, radial flux leakage path.**

I. Introduction

AXIAL flux permanent magnet motors (AFPM) have become a compelling alternative to traditional radial flux permanent magnet motors (RFPMs). Their disc-shaped geometry places the magnetic core and magnets at a larger air-gap area than the conventional RFPM, delivering significantly higher torque and power densities for the same active volume [1]. Their thin, pancake-like form factor allows direct installation in space-constrained systems, such as wheel traction drives, advanced air mobility propulsors, and industrial applications [2]. As electrification accelerates and demand for high-performance AFPM grows, the importance of fast and accurate analysis of AFPM becomes significant.

Accurately predicting the electromagnetic behavior of an AFPM motor requires resolving 3-D flux features, such as radial leakage paths, axial end effects, and skewed fringing fields. Full 3-D finite element analysis (FEA) can capture these phenomena and is therefore regarded as the highest fidelity tool for performance verification. However, utilizing 3D FEA in a design process is limited because it requires an excessive amount of computation. Therefore, an alternative design method for AFPM has been introduced.

Researchers have widely adopted the quasi-3-D (quasi-3D) model for this purpose. The quasi-3D model represents the AFPM geometry in a flattened, 2-D equivalent form [3]. However, as the conventional quasi-3D model is computed in the 2-D plane, it does not fully capture critical effects. Such effects include radial flux leakage and end coil inductance [4], leading to discrepancies in the analysis results. Various strategies have been investigated to mitigate these discrepancies, including the use of magnetic equivalent circuits and analytical methods [5], [6], [7].

On the other hand, Ahn et al. [8] demonstrated a method of using a single-step 3-D analysis to analyze an AFPM through flux linkage. In this way, 3-D flux features are accounted for in a shorter computation. However, this technique is only viable when the flux linkage is sufficiently sinusoidal. Meanwhile, Jung et al. [9] and Jung [10] show how omitted flux leakage paths in 2-D analysis can be integrated by mathematically adjusting the permeance, thereby improving overall accuracy without incurring additional computational burden. The authors performed this study for an RFPM with a short axial length, which experiences similar 3-D flux leakage. However, such methodology has not been applied to AFPM yet.

In response to such considerations, we propose an improved quasi-3D model that integrates the radial flux leakage path by incorporating the permeance of the radial leakage path into the 2-D analysis. As a result, the improved quasi-3D model achieves better correlation with 3D FEA while maintaining the computational efficiency of a conventional quasi-3D model with only two divisions of planes. In this article, the target motor and the method used to incorporate radial flux leakage are presented in Section II. In Section III, the performance of the conventional quasi-3D and improved quasi-3D methods

Received 19 July 2025; accepted 28 September 2025. Date of publication 1 October 2025; date of current version 13 July 2026. Corresponding author: M.-S. Lim (e-mail: myungseop@hanyang.ac.kr).

Color versions of one or more figures in this article are available at https://doi.org/10.1109/TMAG.2025.3616439.

Digital Object Identifier 10.1109/TMAG.2025.3616439

TABLE I
MOTOR SPECIFICATION

Specification	Value
Motor Type	Single-stator, dual-rotor AFPM
Pole / Slot	8 / 12
Magnet residual flux density at 20°C	1.41 T
Stator / Rotor core material	35PN230 / S45C
Max Current	50 A_{rms}

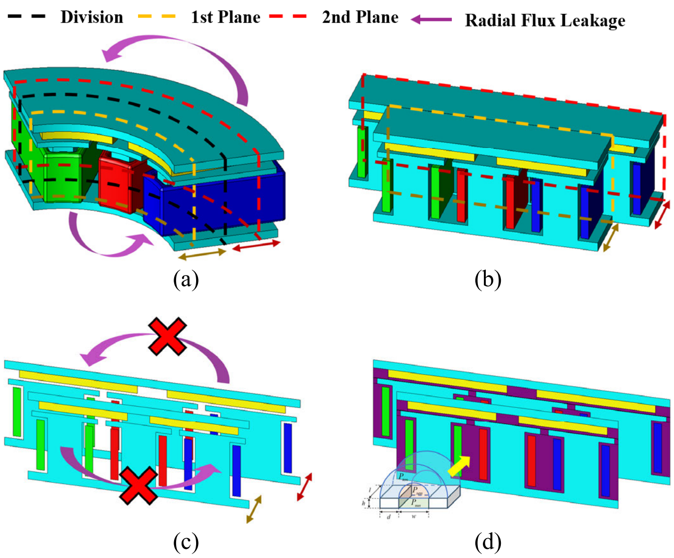

Fig. 1. AFPM analysis methods. (a) Three-dimensional model. (b) Equivalent linear model. (c) Conventional quasi-3D model. (d) Improved quasi-3D model.

is compared with that of the 3D FEA for various outputs. Section IV compares FEA results with the experimental results for the validation of the process.

II. ANALYSIS METHODS OF AN AFPM

A. Motor Specifications

The target motor is a single-stator, dual-rotor AFPM. The motor is controlled with zero d-axis current, that is, all current is induced in the q-axis. In order to prove the wide range of operation points, performances are compared in most of the current range. In this way, the accuracy evaluation of the improved quasi-3D model guarantees a broader validation. Table I summarizes the key specifications, including material properties and maximum stator current.

B. Conventional Analysis Methods

Fig. 1 shows various methods for the analysis of an AFPM. The 3D FEA shown in Fig. 1(a) provides the highest fidelity representation of the AFPM geometry. It provides performance estimates closest to real-world operation. However, it requires extensive computation time due to the large number of meshes. This disadvantage hinders the usage of 3D FEA in computationally intensive processes, such as optimization.

In order to overcome the excessive computation requirement of the 3D FEA, the 2D FEA-based quasi-3D analysis is suggested. The construction of a quasi-3D model follows. The geometry is first transformed into a linear model that represents the 3-D model in most respects, as shown in Fig. 1(b).

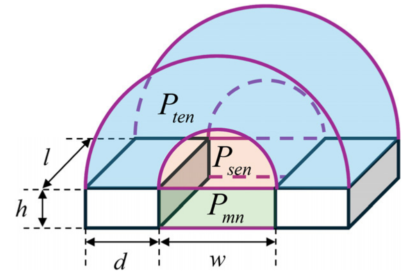

Fig. 2. Permeance calculation for radial leakage flux.

The model is flattened according to the length of the center line of each division. The length between the outer radius and inner radius is divided into a desired number of divisions, which is used as the thickness of each plane. This model can be converted into a 2-D-compatible, conventional quasi-3D model, as depicted in Fig. 1(c), since it shares the same topology throughout the section. The number of divisions required to create an equivalent linear model can vary depending on the need for accuracy and computation time. More division could suggest better accuracy but at the cost of more computation [11]. This article divides the model into two and ten planes to verify the tradeoff between accuracy and computation efficiency. This conventional method, however, inherently neglects the radial flux leakage present in the original 3-D model, imposing a fundamental limit on accuracy improvement, regardless of the number of divisions

$$P_{\mathrm{mn}} = \mu_o \frac{hl}{w} \tag{1}$$

$$P_{\mathrm{ten}} = \mu_o \frac{l}{\pi} \ln\left(1 + \frac{2d}{w}\right) \tag{2}$$

$$P_{\mathrm{sen}} = \mu_o 0.264 l \tag{3}$$

$$\mu_{\mathrm{re}} = \frac{P_{\mathrm{mn}} + P_{\mathrm{sen}} + P_{\mathrm{ten}}}{P_{\mathrm{mn}}}. \tag{4}$$

C. Improved Quasi-3D

To address the limitation of not accounting for radial leakage flux in the conventional quasi-3D model, we propose an improved quasi-3D model, as shown in Fig. 1(d). Each of the two planes now features a dedicated radial flux leakage path—one for the inner side and another for the outer side—by calculating an effective relative permeability μ_{re}. μ_{re} is calculated according to the expressions in (1) through (4), and μ_o stands for the permeability of the air [12]. A graphical demonstration of each leakage path is shown in Fig. 2. The main leakage path's permeance, which remains even after the conventional quasi-3D conversion process, is represented as P_{mn}. The calculation of P_{mn} is given in (1). Radial leakage paths are modeled as a semicircular cylinder (P_{sen}) and a half annulus (P_{ten}). The permeance of each path is expressed in (2) and (3), respectively. Then, the new permeability μ_{re}, accounting for the radial flux leakage path into the 2-D domain, is obtained according to (4). By obtaining μ_{re}, the radial flux leakage path omitted in the conventional quasi-3D model is reflected in the 2-D domain.

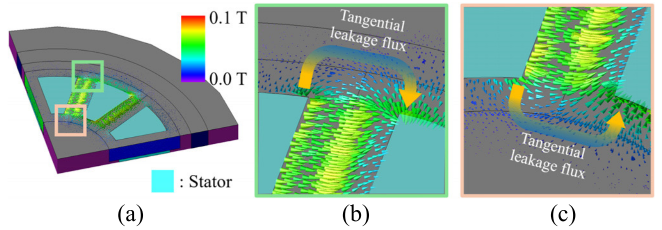

Fig. 3. Stator flux leakage path at 50 A_{rms}. (a) Cut plane of the 3-D model. (b) Tangential leakage around the outer radius. (c) Tangential leakage around the inner radius.

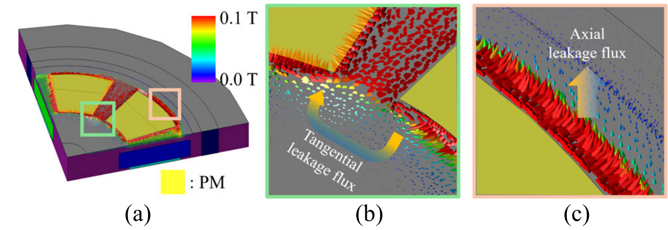

Fig. 5. Rotor flux leakage path at 50 A_{rms}. (a) Cut plane of the 3-D model. (b) Tangential leakage around the inner radius. (c) Axial leakage around the outer radius.

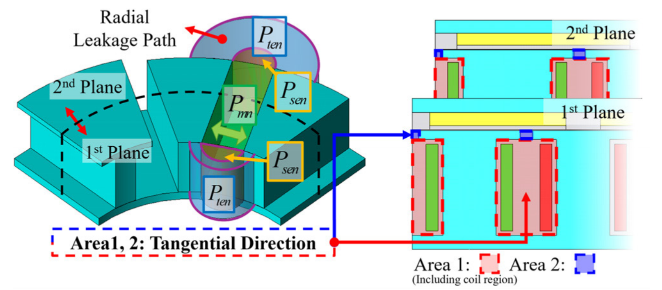

Fig. 4. Concept of radial leakage path, plane division, and separated area in the stator.

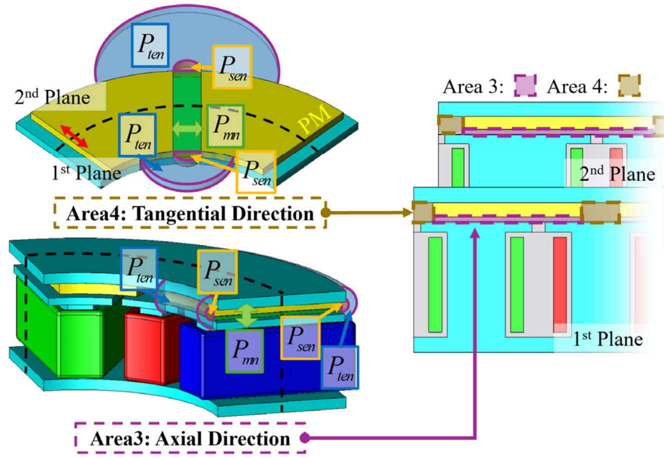

Fig. 6. Concept of radial leakage path, plane division, and separated area in the rotor.

To ensure accuracy, μ_{re} is calculated for four different regions based on the motor's geometry. As the stator and rotor show distinct leakage paths, the direction of the assumed radial leakage paths differs. The stator has two areas designated according to geometrical change. Area 1 is in the slot area where the stator coil is inserted. The direction of the leakage path is determined to be tangential to the surface, as the leakage mainly exists in the tangential direction, as shown in Fig. 3.

Then, the leakage path and direction are assumed as displayed in Fig. 4. The leakage path of the inner and outer radial space is allocated to each plane of the improved quasi-3D model. To visualize the main leakage path (P_{mn}) more clearly, the tooth tip and coil are removed from the figure, and the radial leakage paths are depicted accordingly. μ_{re} is also applied to the coil area in area 1. The same analogy goes to area 2, which is also known as the slot opening area of the stator tooth tip.

The rotor, on the other hand, has two distinct radial-leakage components that must be modeled separately. As shown in Fig. 5(b), the area between the permanent magnet (PM) has tangential leakage flows that circumferentially flow through the radial space. Axial leakage, in contrast, occurs within the magnet, as shown in Fig. 5(c). The flux is protruding in an axial direction, thus becoming a fringing and leakage passage. Although both phenomena are confined to the radial space, their different directions need to be accounted for separately. Fig. 6 shows how the tangential and axial leakage paths are defined and applied to the improved quasi-3D model. The improved quasi-3D model assigns an independent radial leakage branch to each path—the tangential branch is placed in the air region between the PM. In contrast, the axial branch is embedded under the PM, thereby capturing rotor leakage effects without sacrificing computational efficiency.

TABLE II
EFFECTIVE RELATIVE PERMEABILITY OF EACH REGION

Area	1st Plane μ_{re}	2nd Plane μ_{re}
1	1.373	1.447
2	1.155	1.169
3	1.140	1.140
4	1.776	1.992

The resulting μ_{re} values are provided in Table II. This approach enables the radial flux path to be projected into the 2-D-based improved quasi-3D analysis, allowing the model to capture radial leakage effects without requiring additional computation.

III. FEA Performance Comparison

In this section, the performance of estimating the 3D FEA is compared for various quasi-3D methods. For a comprehensive evaluation, the conventional quasi-3D analysis is performed for both two-plane and ten-plane models, confirming that the proposed two-plane approach surpasses the finely divided conventional quasi-3D model in accuracy. Target performance includes average torque, torque ripple, induced voltage, and inductance. The validation is conducted for 20–50 A_{rms}, which is the main operation region for the motor.

A. Torque Characteristics

Fig. 7 shows that all the quasi-3D analysis methods predict the average torque with an acceptable degree of accuracy.

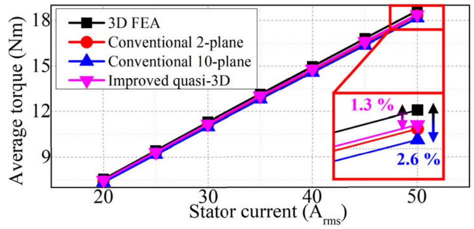

Fig. 7. Comparison of the average torque in various stator currents.

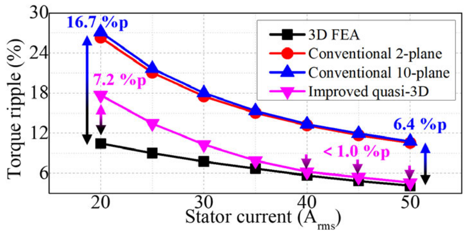

Fig. 8. Comparison of the torque ripple in various stator currents.

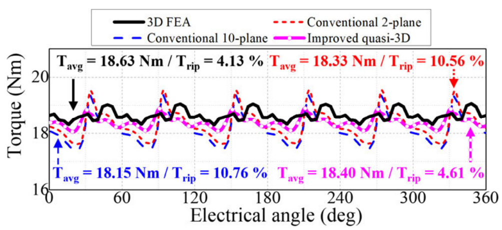

Fig. 9. Torque waveform of each analysis method at 50 A_{rms}.

Still, the proposed method demonstrates the highest level of precision, with an error of only 1.3%. The prediction error of the other models remains within a narrow margin of 3% relative to the 3D FEA results, yet it is larger than that of the proposed method.

Regarding torque ripple, however, the estimation accuracy of the analysis models shows significant variation. Fig. 8 illustrates that the conventional quasi-3D models consistently overestimate the torque ripple, while the proposed method's prediction aligns closely with the 3D FEA results. At a current of 20 A_{rms}, the conventional two-plane and ten-plane models exhibit large errors of 15.8%p and 16.7%p, respectively; in contrast, the proposed method's error is lower at 7.2%p. This enhanced accuracy is maintained at higher currents as well; at 50 A_{rms}, the errors of the conventional methods remain above 6.4%p, while the proposed method's error is reduced to less than 1.0%p. This result demonstrates that accurate torque ripple prediction is highly dependent on the 3-D leakage flux, which is effectively accounted for in the proposed model.

Fig. 9 shows the waveform and related values of torque obtained by each analysis method at 50 A_{rms}. T_{avg} and T_{rip} represent the average torque and torque ripple, respectively. The conventional quasi-3D methods' waveforms have similar waveforms, even though their divisions have a five times difference. The 3D FEA and improved quasi-3D methods show the most comparable results. This result confirms that the improved quasi-3D method is suitable for predicting 3D FEA torque.

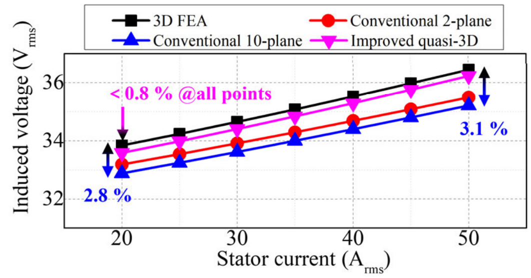

Fig. 10. Comparison of the fundamental component of the induced voltage in various stator currents.

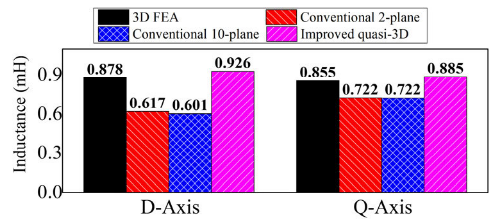

Fig. 11. Comparison of the D- and Q-axes inductance at 20 A_{rms}.

B. Induced Voltage

The comparison of the fundamental component of the induced voltage, presented in Fig. 10, further highlights the accuracy of the proposed method. The conventional ten-plane model shows the largest discrepancy, with a prediction error of approximately 2.8%–3.4% across the operating range. The conventional two-plane model provides a more accurate estimation, with its error remaining in the range of 1.9%–2.6%. The proposed method demonstrates the highest fidelity, consistently maintaining its error below 0.8% across the entire current range and aligning very closely with the 3D FEA results. It is also noticeable that as the current increases, the error of conventional models slightly increases, whereas the proposed model shows the opposite trend. This result indicates that the proposed method's compensation for leakage flux is crucial for accurately predicting the main flux linkage, which directly determines the induced voltage.

C. Inductance

The performance comparison of D- and Q-axes inductances is presented in Fig. 11. For accurate estimation of the inductance, the incremental inductance method [13] is used at the 20 A_{rms} stator current condition. The conventional models show an underestimation of inductance, which is particularly severe for the D-axis, where the errors reach approximately 30%. In contrast, the proposed method's results are significantly closer to the 3D FEA values, showing a slight overestimation with errors of 5.6% for the D-axis and 3.5% for the Q-axis.

D. Computation Cost

Table III shows the computation cost of each analysis method for one electrical period. Time and element number are added together for multi-plane models. The analysis is performed in JMAG using an Intel Core i7-13700K processor

TABLE III
COMPUTATION COST OF EACH ANALYSIS METHOD

Analysis Method	Time (s)	Elements
3D FEA	2,771	361,798
Conventional quasi-3D 2-plane	21	92,617
Conventional quasi-3D 10-plane	137	496,644
Improved quasi-3D	22	92,617

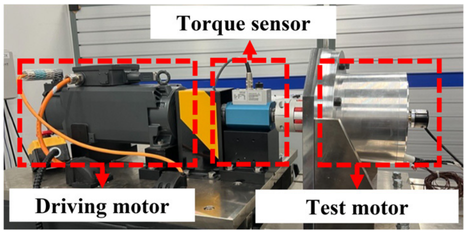

Fig. 12. Experimental setup for AFPM.

with 64 GB of memory. Three-dimensional FEA exhibits the longest computation time, approximately 125 times that of the improved quasi-3D method. Although the conventional ten-plane model utilizes more elements than the 3D FEA, its computation time is shorter as it is a 2-D-based analysis. This comparison confirms that the proposed improved quasi-3D method requires no additional computational cost relative to the conventional two-plane model.

Overall, the comprehensive comparison validates that the improved quasi-3D method provides superior accuracy across all performance metrics. This enhanced fidelity stems from its direct consideration of radial leakage flux paths, which is crucial for accurately estimating torque ripple and inductance. In contrast, the conventional approach exhibits a flaw where increasing model divisions to ten planes instead degrades accuracy. This occurs because radial leakage flux is excluded from the quasi-3D model, limiting the potential accuracy improvement. Increasing the number of radial slices merely raises the computational cost without closing the gap to the 3D FEA. Therefore, this study confirms that the proposed method's focus on physical accuracy makes it a reliable tool for AFPM motor design.

IV. EXPERIMENTAL VERIFICATION

A. Test Configuration

To validate the performance of the proposed analysis method, the designed AFPM motor was manufactured and tested. Fig. 12 shows the experimental setup, which consists of the test motor, a driving motor, a torque sensor, and a control system. The test motor is mechanically coupled to the driving motor, which serves as a dynamic load. A non-contact torque sensor (Kistler 4503B) is installed between the two motors to measure the output torque, with a range of 50 Nm and an accuracy of 0.05%. The phase currents and voltages of the test motor are measured using a power analyzer (Yokogawa WT1804E) and an oscilloscope. The experiments were conducted at an ambient temperature of approximately 25 °C.

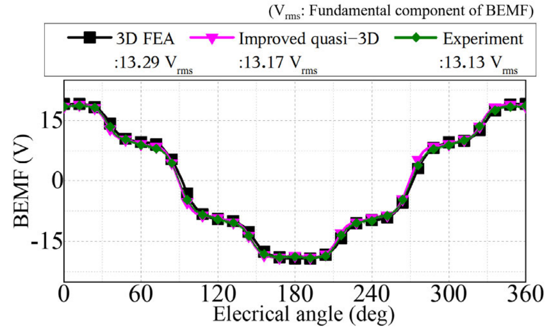

Fig. 13. Comparison of back electromotive force at 1000 r/min with experimental results.

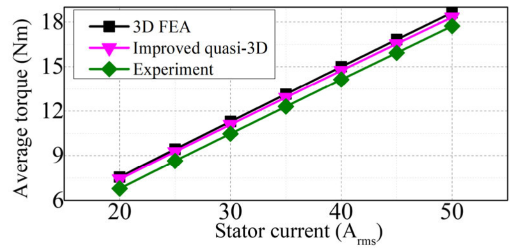

Fig. 14. Comparison of average torque in various stator currents with experimental results.

B. Back Electromotive Force

The no-load back-electromotive force (BEMF) at 1000 r/min is compared for validation, as presented in Fig. 13. A high degree of agreement is observed not only in the RMS values but also in the overall waveform shapes among the 3D FEA, the proposed model, and the experimental results. The error for the proposed model is only 0.9% relative to the 3D FEA and 0.3% relative to the experimental measurement. The 3D FEA also demonstrated agreement with the experimental result, showing an error of only 1.2%. This correlation, in both magnitude and shape, confirms the proposed model's ability to predict the motor's BEMF accurately.

C. Average Torque

Fig. 14 presents a comparison of the average torque obtained from the simulation models and experimental measurements, which are conducted to validate the analysis results. A consistent offset of approximately 0.8 Nm is observed between the experimental data and the simulation predictions, resulting in measured torques that are lower than the 3D FEA results at all current points. Despite this offset, the slope of the experimental torque curve shows good agreement with the slopes of both the 3D FEA and the improved quasi-3D model. Therefore, the strong correlation between the predicted and measured torque–current characteristics validates that the proposed analysis method is an effective tool for predicting the motor's performance.

V. CONCLUSION

This article presented an improved quasi-3D model for AFPM motors that considers the radial flux leakage path in the 2-D analysis. By mathematically calculating the permeance of these leakage paths and applying it as an effective relative permeability within the 2-D domain, the model overcomes a primary source of inaccuracy inherent in conventional quasi-3D approaches. Comparative analysis demonstrated that the proposed improved quasi-3D analysis provides better agreement with 3D FEA results, with only a two-plane division in the average torque, torque ripple, induced voltage, and inductance estimation when compared to both two-plane and ten-plane conventional models. The study also revealed that increasing the number of divisions in a conventional model does not guarantee higher accuracy and could instead increase errors. Experimental verification with a manufactured AFPM motor prototype further validated the proposed method. This improvement comes without increasing computational cost, making the proposed method a promising tool for more efficient and accurate AFPM motor design and optimization.

References

[1] N. Gadiyar, J. Van Verdeghem, and E. L. Severson, "A review of axial flux permanent magnet machine technology," *IEEE Trans. Ind. Appl.*, vol. 59, no. 4, pp. 3920–3933, Jul. 2023.

[2] Z. Hao, Y. Ma, P. Wang, G. Luo, and Y. Chen, "A review of axial-flux permanent-magnet motors: Topological structures, design, optimization and control techniques," *Machines*, vol. 10, no. 12, p. 1178, Dec. 2022.

[3] A. Parviainen, M. Niemelä, and J. Pyrhönen, "Modeling of axial flux permanent-magnet machines," *IEEE Trans. Ind. Appl.*, vol. 40, no. 5, pp. 1333–1340, Sep. 2004.

[4] V. Puttaraj, S. T. Lundmark, and T. Thiringer, "Moving from a 3D axial flux machine model to 2D considering the impact of end leakage flux," in *Proc. Int. Conf. Electr. Mach. (ICEM)*, Sep. 2024, pp. 1–7.

[5] O. Maloberti et al., "3-D–2-D dynamic magnetic modeling of an axial flux permanent magnet motor with soft magnetic composites for hybrid electric vehicles," *IEEE Trans. Magn.*, vol. 50, no. 6, pp. 1–11, Jun. 2014.

[6] J. Zhu, S. Li, X. Guo, H. Nan, and M. Yang, "Analytical calculation of leakage permeance of coreless axial flux permanent magnet generator," *COMPEL-Int. J. for Comput. Math. Electr. Electron. Eng.*, vol. 41, no. 1, pp. 172–186, Jan. 2022.

[7] X. Sun, L. Wang, X. Fan, D. Li, R. Qu, and J. Chen, "A quasi-three-dimensional magnetic equivalent circuit model of yokeless and segmented armature axial flux motors considering radial segmentation magnetic coupling," in *Proc. IEEE Transport. Electrific. Conf. Expo., Asia Pacific (ITEC Asia Pacific)*, Haining, China, Oct. 2022, pp. 1–6.

[8] J.-M. Ahn, H.-K. Yeo, J.-Y. Kim, D.-H. Lee, and D.-K. Lim, "Evolved quasi-3D analysis method for analysis cost reduction of axial flux permanent magnet motor," *IEEE Access*, vol. 11, pp. 141241–141250, 2023.

[9] J.-W. Jung, H.-I. Park, J.-P. Hong, and B.-H. Lee, "A novel approach for 2-D electromagnetic field analysis of surface mounted permanent magnet synchronous motor taking into account axial end leakage flux," *IEEE Trans. Magn.*, vol. 53, no. 11, Nov. 2017, Art. no. 8208104.

[10] J.-W. Jung, "Design of torque density improved spoke-type IPMSM for electric brake booster take into account axial leakage flux," *IEEE Trans. Transport. Electrific.*, vol. 10, no. 2, pp. 3538–3549, Jun. 2024.

[11] K.-H. Kim and D.-K. Woo, "Novel quasi-three-dimensional modeling of axial flux in-wheel motor with permanent magnet skew," *IEEE Access*, vol. 10, pp. 98842–98854, 2022.

[12] J. F. Gieras, *Permanent Magnet Motor Technology: Design and Applications*, 3rd ed., Boca Raton, FL, USA: CRC Press, 2009, p. 328. [Online]. Available: https://www.crcpress.com

[13] T. W. Nehl, F. A. Fouad, and N. A. Demerdash, "Determination of saturated values of rotating machinery incremental and apparent inductances by an energy perturbation method," *IEEE Power Eng. Rev.*, vols. PER-2, no. 12, pp. 28–29, Dec. 1982.